Reliability-Based Damage Tolerance Framework for Achieving Highly Reusable Launch Systems

Leland Shimizu[1], Vinay Goyal[2], Nikolas Nordendale[3], Xueyong Qu[4]
The Aerospace Corporation, El Segundo, California, 90245, USA

Jon Strizzi[5]
Space Systems Command, United States Space Force, El Segundo, CA

Deneen Taylor[6]
NASA Langley Research Center, Hampton, VA

The United States Space Force and NASA are exploring approaches that enable rapid launch response via highly reusable launch systems. One hindrance to achieving high reusability is the inability to meet damage tolerance requirements. To this end, a framework for applying reliability-based damage tolerance to space structures is presented. The reliability-based approach employs probabilistic distributions of key input variables such as material properties, geometry, loads, inspection probability, and defect characteristics to predict hardware reliability for the planned mission life. The probabilistic variables needed to perform the reliability assessments are defined and recommendations on how to collect the required data are provided. Several example problems illustrate the implementation and execution of this approach.

I. Introduction

The United States Space Force and NASA are exploring approaches that enable rapid response via highly reusable launch systems. One hindrance to achieving high reusability is the inability to meet damage tolerance requirements. An approach to achieving high reusability could be employing a reliability-based analysis. Reliability analysis for damage tolerance has been applied in the nuclear, aircraft, and naval industries.

One common damage tolerance approach used in the aerospace industry is to perform an assessment assuming an initial flaw exists in the hardware. The size of the initial flaw is chosen to be greater than or equal to the minimum flaw size which can be detected using non-destructive evaluation (NDE) with a 90% probability of detection at a 95% confidence level (P90/C95) [1]. If the characteristics of the flaw are unknown, the analysis must consider the worst-case location(s) and orientation(s) while accounting for interaction effects from adjacent or nearby flaws. In the case where flaw characteristics are known, the assessment uses those characteristics. Average values of fracture toughness and fatigue crack growth rates are used in the assessment. The part with this initial flaw must survive at least four times the predicted service life. The factor of four in the life assessment is used in the space industry to account for

---

[1] Sr. Member of Technical Staff, Structures Department
[2] Technical Fellow, AIAA Associate Fellow
[3] Systems Director, Launch Systems Ops and Development
[4] Engineering Specialist, Structures Department
[5] Director of Engineering, SSC Assured Access to Space, Chief Engineer, ACAT-1D National Security Space Launch Program, Co-Lead for Space Access, Mobility & Logistics (SAML)
[6] NASA Technical Fellow for Structures

dispersions in fatigue fracture properties and provides margin against unstable fracture. In this paper, the approach described above is referred to as deterministic fracture mechanics (DFM) analysis.

Standard P90/C95 flaw sizes for various NDE techniques for use in deterministic damage tolerance assessment are listed in NASA-STD-5009B [2]. These standard flaw sizes were intended to be developed such that 95% of NDE inspectors could achieve a 90% probability of detection with 95% confidence. However, re-analysis of the original data by the NASA Engineering Safety Center uncovered potential issues for select techniques. [3]

A less frequently used approach in the space industry is the probabilistic fracture mechanics (PFM) approach. In the PFM approach, probabilistic distributions describing each relevant input parameter are constructed and used as inputs into a part reliability analysis. The uncertainty in the input variables is propagated through a crack growth analysis to determine the part reliability for the planned mission life.

While PFM analysis is rarely used in the space industry, it has been widely researched by academia [4] and applied in industry [5,6]. In the aircraft industry, the Federal Aviation Administration (FAA) Advisory Circular published guidance on the use of PFM for damage tolerance verification of aircraft engine components [7,8]. Likewise in the nuclear power industry, the Nuclear Regulatory Commission (NRC) published guidance on the use of PFM for reactor and nonreactor license submittals [9,10]. The FAA and NRC both accept PFM analyses as a tool for the qualification and licensing of new designs. The primary challenge with applying PFM to space applications is the low production rates, which means that each hardware that is produced is an extremely invaluable asset. There is insufficient hardware available to characterize flaw distributions throughout the production process. This paper explores the application and challenges in applying PFM to space structures.

II. Challenges and Benefits of a Reliability-Based Framework

There are challenges associated with applying PFM in practice. The estimated reliability depends on the quality of the statistical input parameters. High confidence in the tails of the input distributions is required to accurately predict reliability, which can only be gained from extensive testing. Statistical data for several key variables can be expensive, time-consuming, and difficult to obtain. Finally, the results of probabilistic analyses are prone to misinterpretation, as reliability estimates only consider the probability of failure due to sources of uncertainty included in the analysis. Hardware nonconformances and flight anomalies can cause the realized reliability to be much lower than predicted if they were not considered in the assessment.

Specific challenges in applying PFM in the space industry stem mainly from low production rates. Space hardware tends to be manufactured in small volumes due to high unit value and launch costs. Because fewer units are produced, fewer units are inspected and tested making it harder to infer the rate of occurrence of rare, large defects. The service life of most launch systems is generally shorter than systems in other industries. Most launch vehicles fly once or only a limited number of times, resulting in a small sample size when trying to calibrate reliability models based on observed anomaly rates. Hardware used in other industries are subjected to routine periodic inspections which can be used to continuously calibrate reliability models based on the rate and severity of inspection findings.

Among many benefits of a reliability-based approach is that the risk of fracture failure for a particular component is directly calculated, allowing it to be compared to the allocated risk. Individual component reliabilities can be aggregated to calculate system reliability. PFM can result in a more consistent risk characterization compared to DFM. Risk ratings based on DFM rely on material property crack growth rate variabilities. DFM assumes an initial flaw exists even if not present, so the risk assessment depends on the likelihood of occurrence of a flaw. In well-controlled manufactured hardware where flaws are unlikely and not detected, but assumed to be present in the DFM assessment, the assessment can understate service life predictions In these specific cases, PFM can provide a quantitative basis for risk determination and can be used to extend the service life because there is no longer the need to rely on the presumption that a minimum detectable flaw size exists in the DFM assessment. Note, however, this is not the case for when an actual flaw is detected and considered in the DFM.

In most space applications, inspections are conducted once before launch, while components on highly reusable launch systems could be periodically inspected. PFM can determine the reliability gained by periodic inspection and inform the inspection interval required to achieve a target reliability. In-service inspection can calibrate reliability models, resulting in more accurate reliability estimates and potentially resulting in life extensions over time. To illustrate,

consider a system for which a conservative assumption is made about defect occurrence rate in the initial phases of the design. In production, periodic inspections could find a lower rate of defect occurrence, and the inspections can feed into refining the probabilistic distribution over time. Periodic inspections with no inspection findings can "reset" the service life as well. Similar to aircraft applications, periodic inspections can extend the allowable service life while maintaining high system reliability.

In this work, it is sought to identify and address challenges associated with characterizing required statistical data to enable wider adoption of reliability-based damage tolerance assessments in the space industry. The reliability-based damage tolerance framework is shown in Figure 1. This framework has three main components: quantification of the input variable uncertainty, propagation of the uncertainty through crack growth analysis, and analysis of the output uncertainty. These steps are explained in Sections III, IV, and V respectively.
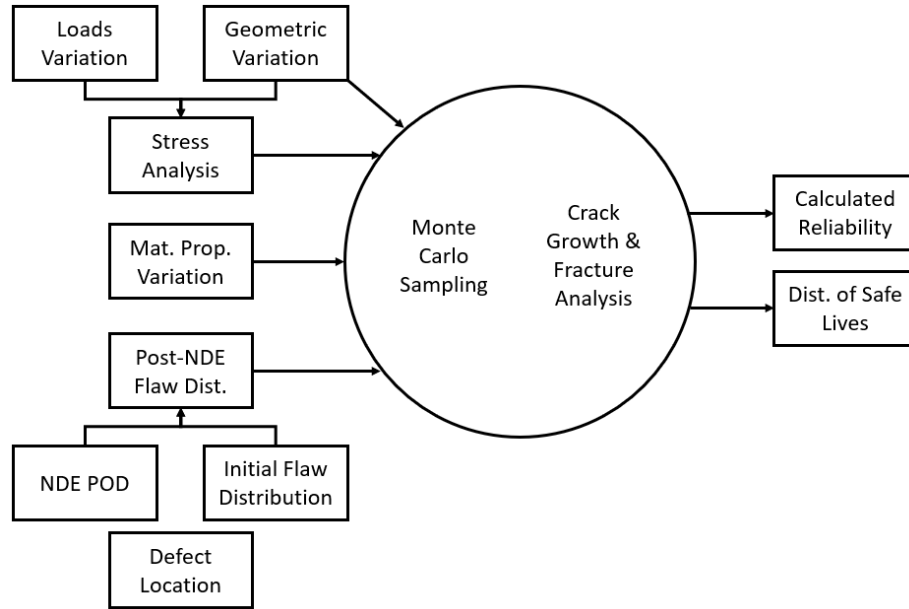
Figure 1. Framework block diagram for reliability-based damage tolerance analysis.

## III.   Quantification of Input Variable Uncertainty

The main input variables for reliability assessment include uncertainty in environments (e.g., loads, temperature), geometry, residual stresses, mechanical properties, strength and fracture toughness, and crack growth rates. Analysis can be further refined by incorporating the initial distribution of flaws within the part and the NDE technique probability of detection (POD), if available.

Not all variables must be modeled as uncertain for every reliability assessment. Both the sensitivity of the fracture analysis to an input variable and the possible uncertainty in that variable should be considered when determining whether to model a variable as uncertain in a reliability assessment. Deterministic sensitivity studies can be performed by varying one input parameter and calculating the corresponding change in predicted safe life to determine if the crack growth analysis is sensitive to that variable. Material selection and manufacturing method primarily control the uncertainty in strength, fracture toughness, crack growth rate, and the distribution of initial flaw characteristics. Uncertainty in geometry can be inferred from engineering drawing tolerances, historical measurements from production runs, and after passing first article inspection. Uncertainty in load and temperatures depends on the subsystem and location. For example, the maximum operating pressure in a metallic pressure vessel is well-controlled, while the pressure in a solid rocket booster may vary from flight-to-flight based upon the formulation and manufacturing of the solid propellant. Random vibration and acoustic loads are often more uncertain than known static loads.

A. Types of Uncertainty

There are two types of uncertainty which must be considered in a reliability assessment: aleatory and epistemic. Aleatory uncertainty arises from the intrinsic randomness of the property in question and is often accounted for by modeling a variable using a distribution. Epistemic uncertainty arises from a lack of knowledge about a property and can be reduced by collecting more data and system knowledge.

One notable source of epistemic uncertainty is the shape of a random variable distribution. When collecting test data, a distribution can be fit to the test data to account for the aleatory uncertainty, represented by the spread in that variable. The confidence in that distribution may be low due to limited sample size. Additional testing could reveal that a different population distribution is a better fit. Statistical software should be capable of fitting a distribution to the test data and accounting for the uncertainty in each of the parameters. Figure 2 shows an example distribution fit with uncertainty applied to geometric measurements.
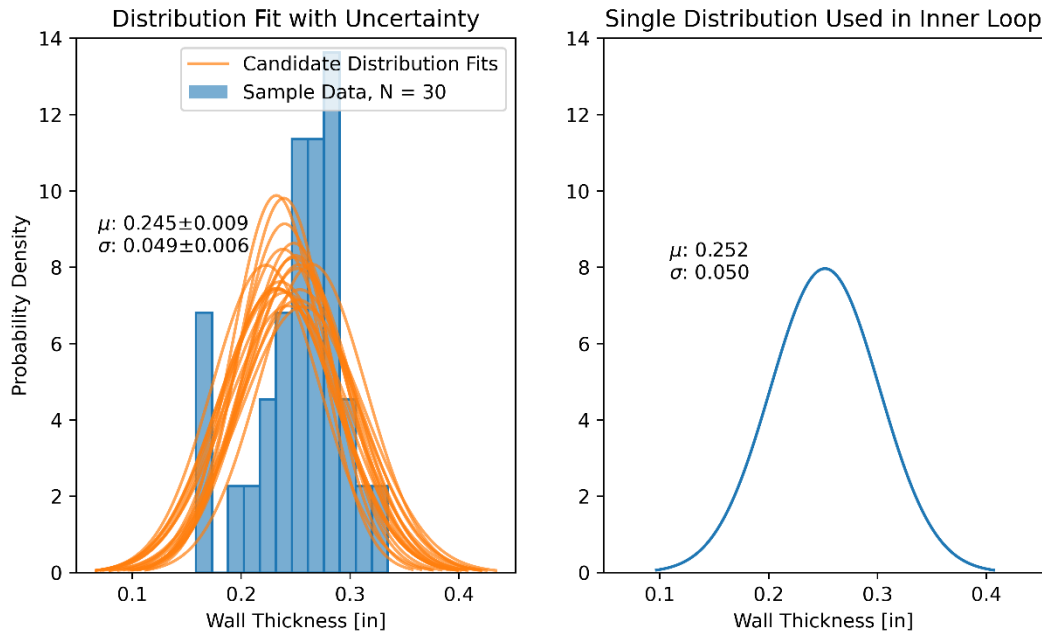
Figure 2. Uncertainty in distribution fit to 30 sample data points.

Maintaining separation between aleatory and epistemic sources of uncertainty through the analysis is recommended because it allows estimating the confidence level corresponding to the reliability results. Further, it allows determination of how uncertainty can be reduced by collecting additional data.

B. Deciding How to Address Uncertainty in Each Variable

Uncertainty in each variable can be addressed in various ways. The first recommended method is to represent the random variable using a parametric distribution and varying the distribution shape and parameters in the outer loop of the reliability analysis. The distribution parameters and their uncertainty can be quantified by using statistical software to fit the distribution to observed data. This method is recommended for variables which the analysis results are most sensitive to.

The second recommended method is to represent the random variable using a distribution with a high level of statistical confidence. An example of this method is using the 95% confidence POD curve in a reliability assessment. This method is useful when data already exist to meet preexisting requirements, or when a distribution is known to be conservative with high confidence but the uncertainty in the distribution is too difficult to quantify.

The final recommended method is to treat the random variable as a constant with a bounding value. Examples of this method include developing the fatigue load spectrum using P99/C90 loads or using P99/C95 material strength and fracture toughness. This method is useful when these data already exist to meet preexisting requirements and the

analysis is not very sensitive to their values. Using bounding constants can introduce conservatism into the analysis, especially when multiple key random variables are treated as a constant with a bounding value.

## C. Collecting Data and Developing Distributions for Random Variables

The number of samples to test and method of data collection will differ for each input variable. The sensitivity of the assessment to a given variable will determine the number of data points which need to be tested to adequately quantify the input uncertainty. Generally, at least 30 data points should be collected for each input variable. The need for additional data collection will emerge from the reliability assessment results if the epistemic uncertainty in distribution fit is properly accounted for and the analysis maintains separation between the epistemic and aleatory uncertainty.

NDE POD Curves

The probability of detection curve represents the rate of detection of flaws of various sizes for one inspection method, as shown in Figure 9. The curve is specific to one inspection method including the equipment and settings used, the material, surface finish, and geometry of the region under inspection.

The POD curve for an inspection method is developed from a POD study, which includes a large range of flaw sizes targeting a qualification flaw size. [2] An inspector uses the NDE procedure to inspect parts containing these flaws and the rate of successful detection is recorded for each flaw size. Then POD curve is obtained by fitting the data with a statistical model.

Compared to assuming an initial flaw exists based on the P90/C95 flaw size, including the full POD curve can greatly impact the calculated reliability. The POD curve accounts for the rate at which flaws smaller than the P90/C95 size are detected and larger flaws are missed, producing the distribution of flaw sizes within a part after inspection. However, using the POD curve in this way requires knowledge of rate of flaw occurrence and distribution of flaw sizes which exist in the part before inspection.
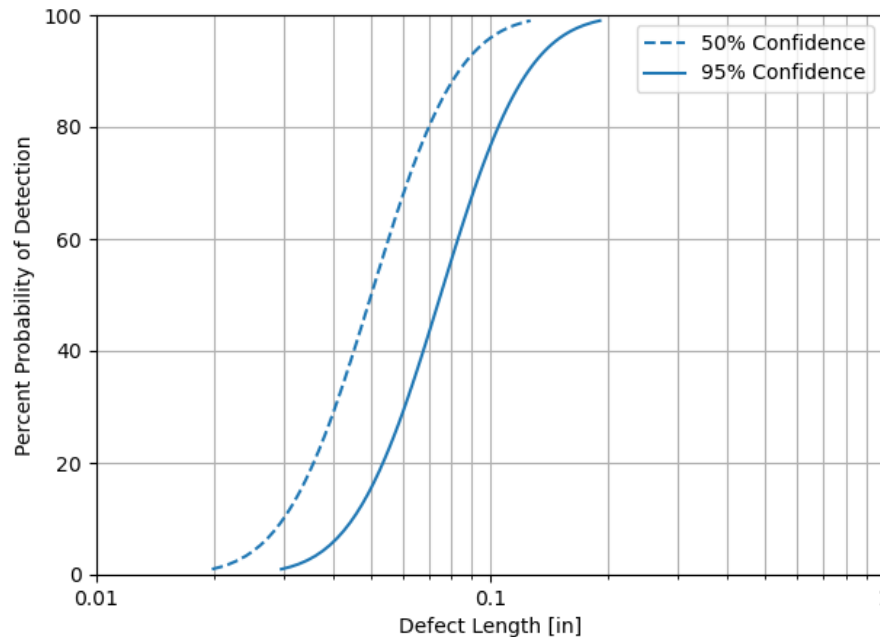
Figure 3. Example NDE POD curves at 50% and 95% confidence levels.

Distribution of Initial Flaws

The distribution of initial flaw characteristics within a part is often the primary variable affecting reliability. Whether a build has a flaw and the size of that flaw dictate how much life will be degraded compared to a pristine build. Four techniques are presented here to estimate the rate of occurrence and size distribution of defects within a component.

Evaluate NDE Finds from Routine Inspections
Many components that are mission critical are subjected to standard NDE inspections prior service. The best effort should be made to estimate flaw size during inspections. A dataset of detected flaw sizes can be built from detected flaws during production runs. In this way, the size distribution and occurrence rate of large flaws can be determined with high confidence. However, the distribution is more challenging to determine for smaller flaws than those detected because the probability of detecting these smaller flaws is low and often not quantified. While smaller flaws are occasionally detected by NDE, the number of undetected flaws in the part is obviously unknown.

Confidence can be gained in the distribution of smaller flaws by determining the full POD curve of the NDE method used during routine inspections. When the probability of detecting small flaws is known, the number of existing undetected flaws can be estimated from the number detected. Whenever a flaw smaller than the qualified P90/C95 flaw size is detected, the number of counts at that size is increased by the reciprocal of the probability of detection for that flaw size. Above the P90/C95 size, only one count per detection is recorded.
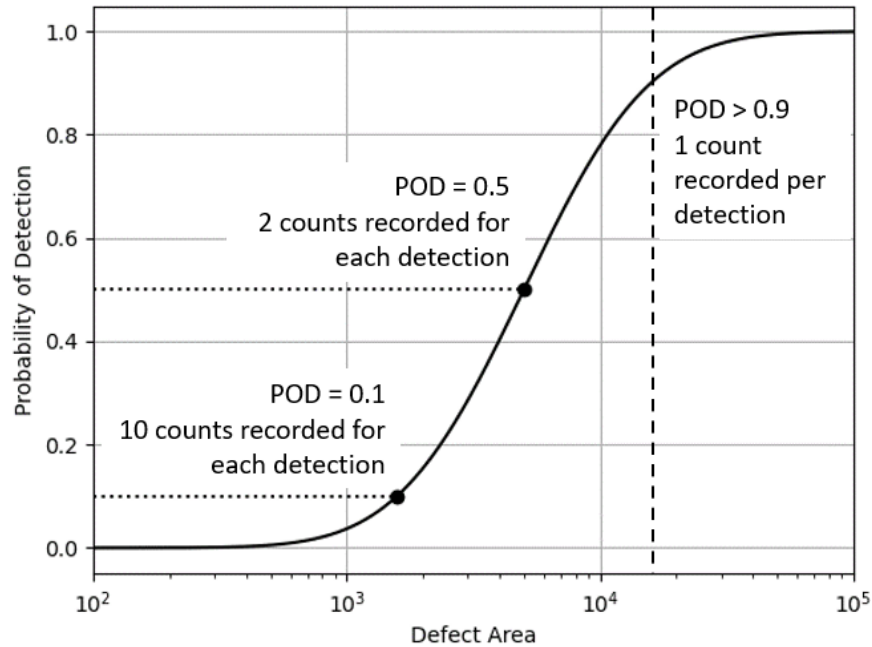

Figure 4. Scaling number of counts based on probability of detection.

Back-Calculate Initial Flaw Sizes from Defects Found In-Service
Reusable launch vehicles are periodically inspected with the goal of finding cracks which may have grown during service. These cracks were smaller than the detection limit prior to service, thus passing inspections; but grew to a detectable size during service. Inhere, the initial flaw size prior to service can be back-calculated by using a crack growth model and the known environments during service. This method of determining the initial flaw size distribution is known as the Equivalent Initial Flaw Size (EIFS) method [11] and has been used to characterize the initial flaw size distribution of aircraft features [12].

This method has the advantage of detecting initial flaws too small to confidently detect during pre-flight inspections. The back-calculation process can introduce errors in the initial flaw size estimate when the dynamic environment is not well characterized, or small crack effects are not accounted for in the calculation.
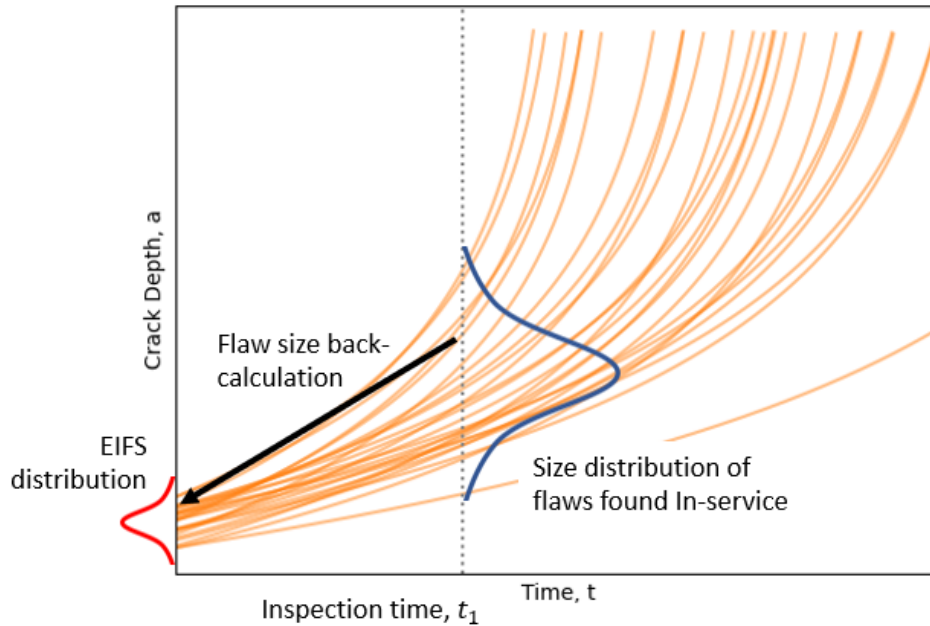
Figure 5. Back calculation of initial flaw sizes from flaws detected in-service.

Perform High-Resolution NDE of a Limited Sample

High-resolution inspection methods such as acoustic or ultrasonic microscopy and X-ray microtomography (microCT), can detect smaller flaws than traditional NDE techniques within localized regions [14, 15]. These methods are useful for determining the occurrence rate and size distribution of the smallest flaws. This method may be necessary for very long mission durations or extreme loads. These methods are extensive and labor-intensive.

Perform Destructive Inspection of a Limited Sample

Destructive inspection methods such as sectioning can determine the size and characteristics of flaws with high confidence. Sectioning is a robust method of characterizing manufacturing defects. However, the method is labor-intensive and expensive.

Using a Combination of Methods

The use of multiple techniques may be required to sufficiently characterize the flaw size distribution. If the goal is to extend the qualified life of a currently flying design, then quantifying the distribution of flaw sizes smaller than the P90/C95 flaw size is likely required. High-resolution NDE and/or sectioning are useful to characterize the population of small and commonly occurring flaws, while routine inspections performed in high volumes are useful to characterize the larger rare flaws.

When combining data from multiple sources to produce the flaw size distribution, it is required that statistical tests be performed to ensure the different techniques assign the same size for the same flaws. This could be achieved by performing two inspection methods on a small sample of hardware containing defects and independently characterizing the defect size with each method. When this method is applied appropriately, the flaws detected from each method can be combined to characterize the flaw size distribution.
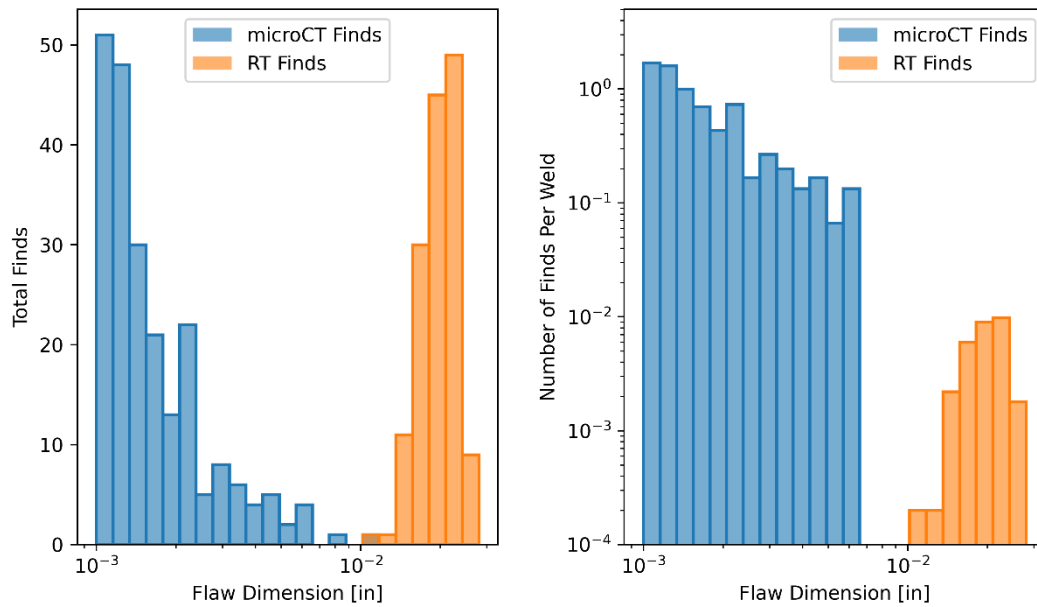
Figure 6. Left: Simulated flaw size data from inspection of 30 welds using microCT and 5000 using radiographic inspection (RT), Right: Data normalized to produce occurrence rate of flaws in welds.

The data on the rate of occurrence and size distribution of flaws can be combined to form the exceedance curve. An example is shown in Figure 7. For each defect size, the exceedance curve encodes the expected number of occurrences of a flaw of that size or greater in a fixed quantity of material or number of parts.
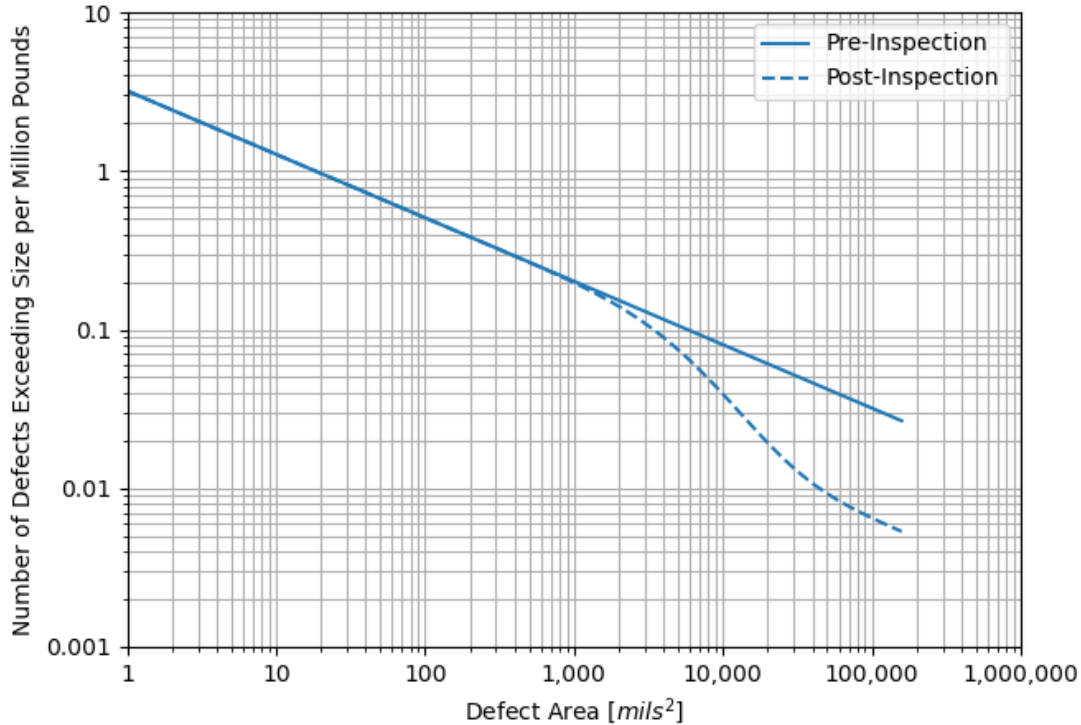
Figure 7. Example exceedance curve which simultaneously represents the rate of occurrence and size distribution of defects within a volume of material. Pre- and post-inspection curves are shown, assuming all parts with detected defects are rejected.
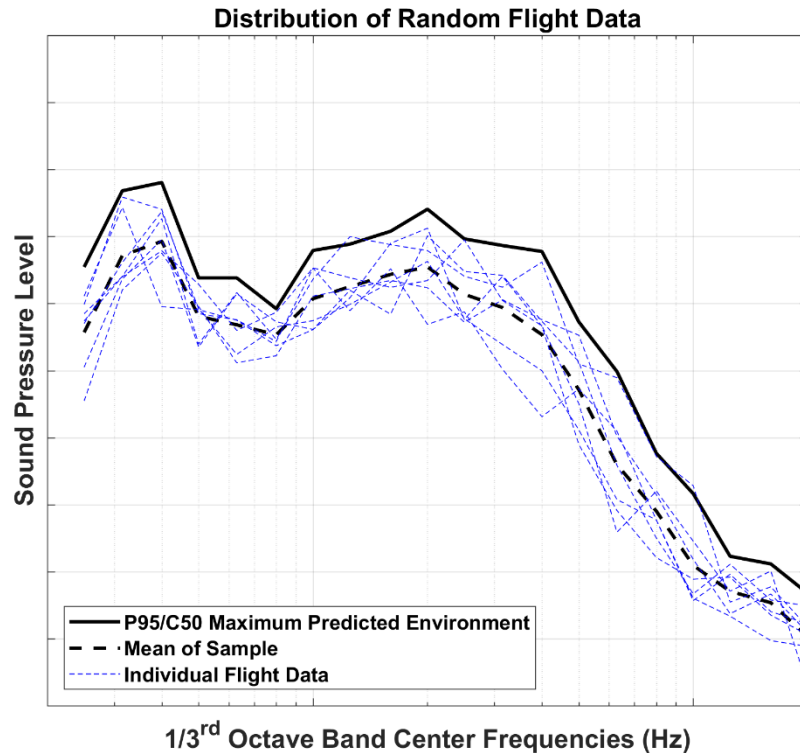
D. Loads and Environments

The importance of including load variation depends on the system which the part belongs to and the environment in which it operates. For example, pressurized components with stresses dominated by well-regulated pressure cycles likely do not benefit from including the small variability in pressure. The importance of load variation in other structural components depends on the proportion of the cyclic stress which results from predictable loads such as static components of engine loads and controlled internal pressure versus more variable sources such as vibration, acoustics, and aerodynamic loads.

Uncertainty in loads can be recovered from coupled loads analysis (CLA) and vibro-acoustic analysis (VAA). CLA is often already run using procedure similar to Monte Carlo analysis. Several possible load inputs, known as forcing functions (FFNs), are applied to the dynamic model for each flight event. The differences between these FFNs represents variations in possible loading conditions including aerodynamic loads, engine gimbaling, actuator timings, and other sources of uncertainty. The structural response of the dynamic model to each FFN input is computed and a statistical maximum (often P99/C90) is taken across the responses to produce upper bound loads for stress and fatigue analysis. To produce loads for PFM analysis, instead of computing a maximum response across the FFN cases, a distribution may be fit to the responses.

VAA is a different case. Typically, VAA is performed by first taking a statistical maximum input environment (acoustic pressure or vibration acceleration) at the P95/C50 level, known as the maximum predicted environment. [15] Then, the structural response is computed using a random response analysis, and fatigue loads are derived. The data used to compute this maximum is obtained through flight experience, ground testing, and computer modeling. To apply PFM, instead of developing a statistical maximum environment, a distribution can be fit to the input environment representing the number of decibels above the mean each individual flight environment was. Because VAA models are linear, scaling the input signal by a factor results in the output response being scaled by the same factor so the structural response distribution is the same as the input distribution.

Whether the fatigue load spectrum is derived using CLA, VAA, or a combination of the two, a reasonable way to account for the load uncertainty is to apply a scaling factor to the amplitude of the fatigue spectrum. For loads derived from CLA, the scaling factor will follow a distribution fit to the dynamic model output responses. For loads derived from VAA, the distribution if fit to the dynamic environment input spectrum.

Figure 8. Spread in sound pressure environments used as input to random response analysis for fatigue load derivation.

E. Geometry
Geometric uncertainty results from manufacturing tolerances and measurement uncertainty. Manufacturing variability will result in variable part thicknesses, fillet radii, surface finish, and other characteristics. These variations can drive differences in local stresses, affecting crack initiation time and growth rates.

The distribution of dimensions of key geometric features can be obtained through several methods. Several flight-quality units of the qualified design could be built and measured. This method produces the most accurate distribution for the geometric variables. Another method is to build a bounded distribution using the upper and lower dimensional acceptance criteria. However, this method is susceptible to error as the true distribution of dimensions may be skewed to one side of the tolerance range. Finally, conservative geometry assumptions could be used.

F. Material Properties
Material strength and fracture toughness properties can be measured from standard material tests. Strength can be measured using ASTM E8 while fracture toughness can be measured from ASTM E399 or ASTM E1820. Generally, at least 30 specimens should be tested to build a distribution. These specimens should be distributed within and between material lots to ensure both sources of uncertainty are accounted for.

G. Crack Growth Rates
Crack growth rates can also be measured from standard material tests, for example, ASTM E467. Generally, at least 30 specimens should be tested to build a distribution. These specimens should be distributed within and between

material lots to ensure the variation between lots is captured in the crack growth rate distribution. A reasonable way to model uncertainty in crack growth rate is to model the constants of the crack growth rate model (e.g., the Paris equation) as uncertain input variables and fit distributions to them.
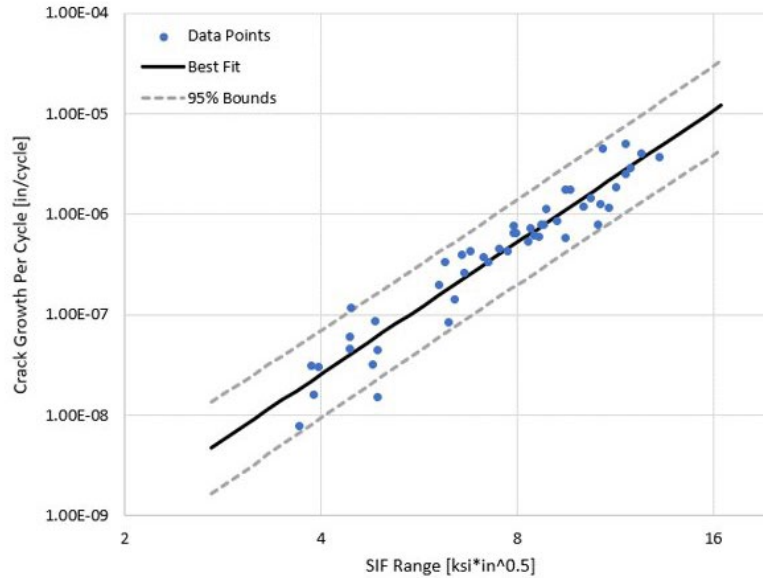

**Figure 9. Example da/dN data with 95% prediction interval.**

IV. Propagation of Uncertainty Through a Damage Tolerance Analysis

A. Monte Carlo Sampling Technique
The method of reliability-based damage tolerance verification presented in this paper employs the Monte Carlo method to propagate uncertainty in the input variables through a crack growth simulation to determine the uncertainty in safe life and the probability of failure. A two-loop Monte Carlo sampling scheme is used to maintain separation between aleatory and epistemic uncertainty sources. [16]

In the inner loop variables of interest such as the initial flaw size, material properties, and loads are sampled from their respective statistical distributions to produce a set of aleatory realizations. Crack growth and fracture analysis is performed for each realization to determine the number of cycles to failure each realization survives. The probability of failure is computed as the fraction of aleatory realizations which fracture within the component's service life.

In the outer loop, the parameters of the statistical distributions, analysis assumptions, and other estimates resulting from a lack of knowledge are varied to produce a set of epistemic realizations. Figure 2 illustrates how distribution parameters are sampled from a distribution fit with uncertainty. The mean and standard deviation of the distribution used in the inner loop are sampled from normal distributions based on the uncertainty in the distribution fit. For each epistemic realization, the inner loop is run to compute the probability of failure (POF) resulting in one POF estimate per epistemic realization. Finally, confidence bounds are computed across all the POF estimates.
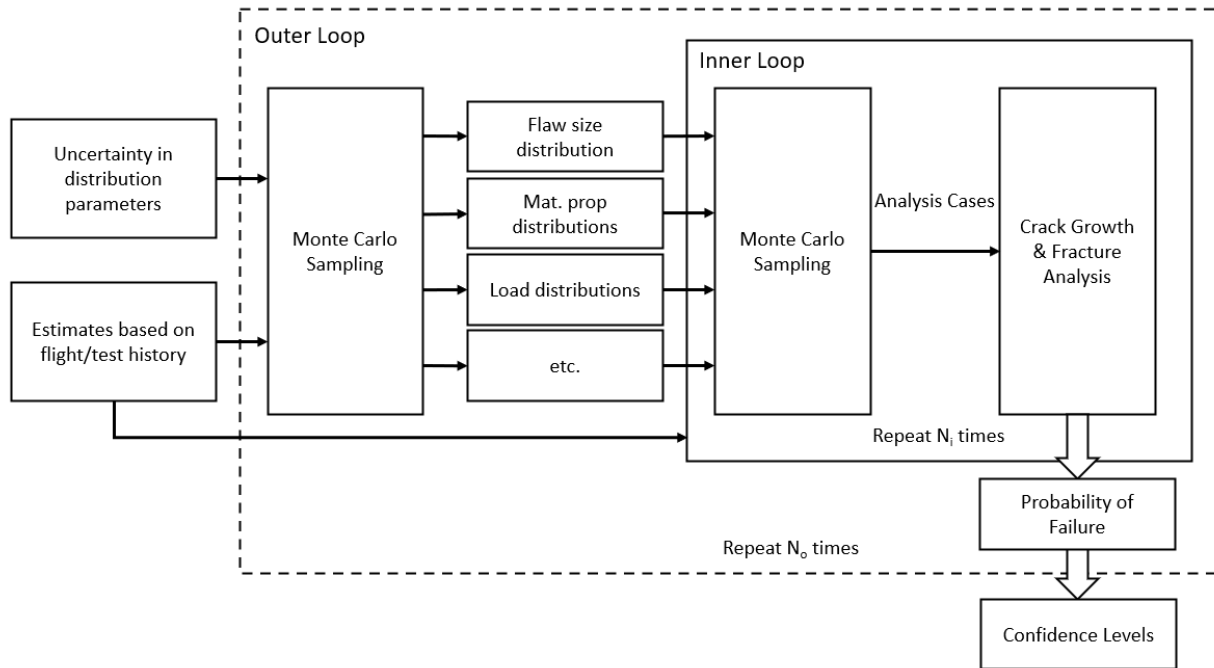
Figure 10. Two-loop Monte Carlo crack growth analysis diagram.

B. Steps to Perform Reliability Assessment Implementing PFM

This section provides the steps required to perform PFM; which includes Loads/Stress Analysis, Sampling, Inspections, and Crack Growth Simulations.

Loads / Stress Analysis
CLA and/or VAA is performed to develop the fatigue spectrum with uncertainty characterized by the CLA output or VAA input. Loads from these models may be obtained at a nearby interface. In that case, finite element analysis or another form of stress analysis should be performed to derive the transfer function between the interface loads and local stresses in the region of interest.

Sampling of Epistemic Random Variables
A sample size for the epistemic realizations, N_e is chosen based on the desired level of confidence in the reliability results. As a rule of thumb, N_e should large enough such at 10 to 100 epistemic realizations fall outside the desired confidence enclosure. For example, if 90% confidence is desired, 100 to 1000 epistemic realizations should be used.

Each epistemic realization includes one value for each variable treated as an epistemic random variable, such as the shapes and parameters of the aleatory random variable distributions. These distribution shapes and parameters are used to construct the distributions used in the inner loop of the analysis.

Sampling of Aleatory Random Variables
A sample size for the aleatory realizations, N_a is chosen based on the desired resolution of the probability of failure. As a rule of thumb, N_a should be chosen such that 10 to 100 aleatory realizations result in failure at the desired reliability level. For example, if 99.99% reliability is desired (1 in 10,000 POF), then 100,000 to 1,000,000 aleatory realizations should be used.

Each aleatory realization represents a hardware build and includes one value for the inputs affecting the damage tolerance analysis, such as fracture toughness, initial flaw size, and crack growth rates. If the number and location of flaws are treated as aleatory random variables, then each aleatory realization will contain one or multiple flaws distributed throughout the hardware.

Inspection Simulation

If the initial flaw size is treated as a random variable, then inspection simulation using the POD curve can be used. For each flaw in each part, the probability of detection is computed from the POD curve. A random number generator is used to determine if that flaw is detected. If it is detected and is determined to be greater than the allowable flaw size, then the part is removed from the PFM analysis, simulating the part's removal from the manufacturing flow. Alternatively, that flaw may be removed from the part to simulate a rework or repair.

If the initial flaws size is not treated as random, then inspection is not simulated. Instead, each part is assumed to contain one initial flaw with its size determined by the P90/C95 flaw size from the NDE procedure.

Crack Growth Simulation

Once the location, size, and stress spectrum are known, the number of service lives survived for each flaw in the part is calculated using a numerical crack growth procedure. The safe life of the part is the minimum life of all flaws in the part. This is repeated for all N_a aleatory realizations. The POF is the proportion of aleatory realizations with safe life below the required service life. POF is calculated using this procedure for each epistemic realization.

V. Analysis of Output Uncertainty

The last step of the reliability assessment is to analyze the uncertainty in the output variables. Within one epistemic realization, each aleatory realization produces a different estimate of the safe life. These estimates can be numerically integrated to produce a probability of failure CDF. Each point on the probability of failure CDF represents the probability that the part has failed before the specified life on the x-axis. Each epistemic realization produces a different probability of failure CDF, which can be plotted together on the same axes to see the effect of the epistemic uncertainty. Finally, the probability of failure estimates from each epistemic realization can be taken at a given life (i.e., number of cycles or flights) and plotted as a histogram to show the probability of failure at that life with a given level of confidence. This process is shown in Figure 11.
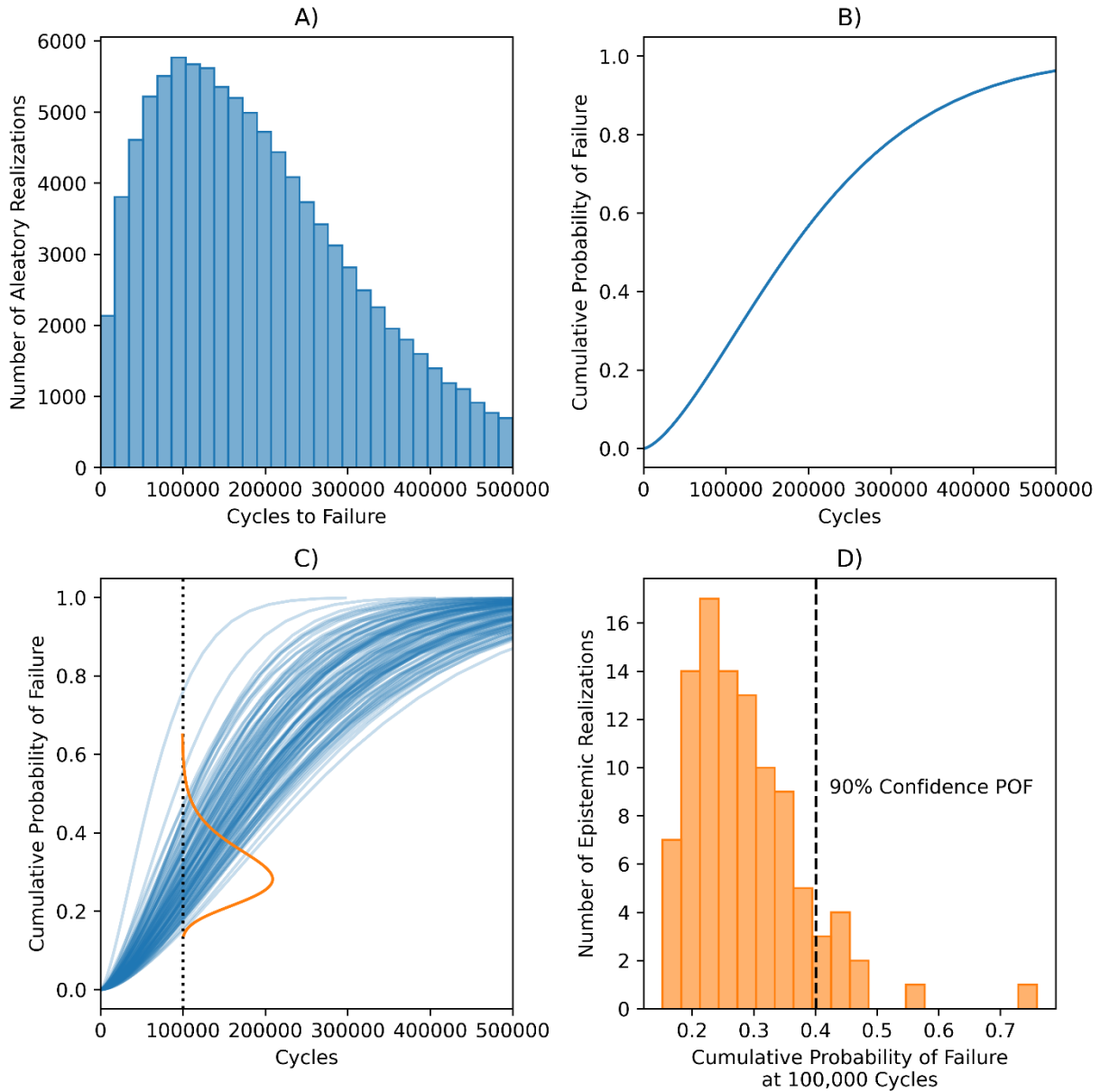
Figure 11. Analysis of output uncertainties. A) shows a histogram representing the cycles to failure of each sample within one epistemic realization. B) shows the probability of failure CDF across one epistemic realization. C) shows the probability of failure CDFs for 100 epistemic realizations. D) shows a histogram representing the probability of failure estimates from all 100 epistemic realizations at 100,000 cycles. The probability that the part fails before 100,000 cycles is 0.4 with 90% confidence.

The effect of epistemic uncertainty on the results can be determined from the probability of failure CDFs. Large spread between the individual CDFs means that the epistemic uncertainty in the input variables has a large effect on the output uncertainty. If this spread is too large such that the reliability estimated at an appropriate confidence level does not meet requirements, then the epistemic uncertainty must be reduced by performing additional testing and data collection.

VI. Examples

A. Reliability Analysis of a Plumbing Section Subjected to Random Vibration Environments

The reliability-based damage tolerance assessment method was demonstrated to predict the probability of failure of a plumbing tube within the propulsion subsystem of a reusable launch vehicle subjected to random vibration environments. Real testing was not performed to develop the input variable distributions, so these distributions are used for the purposes of this numerical example only. The tube wall thickness, crack growth rate, vibration load amplitude, and initial flaw size were treated as random variables. Inspection simulation was also performed to simulate the removal of units with detectable cracks from the production flow. Uncertainty in these variables was propagated through a two-loop Monte Carlo crack growth analysis to determine the probability of failure after 10 to 50 flights.
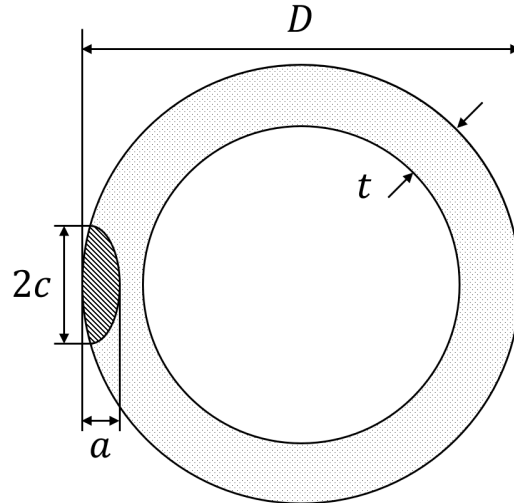
Figure 12. Diagram showing cross section of tube analyzed in example assessment.

The tube in this assessment is made of Ti 3Al-2.5V material and has an outer diameter of 0.25 in with a nominal wall thickness of 0.028 in. Uncertainty in the wall thickness was modeled using a truncated normal distribution with a mean of 0.028 in and a standard deviation of 0.002 in. To model epistemic uncertainty arising from a limited sample size, the distribution mean was modeled using a normal distribution with a standard deviation of 0.0008 in.
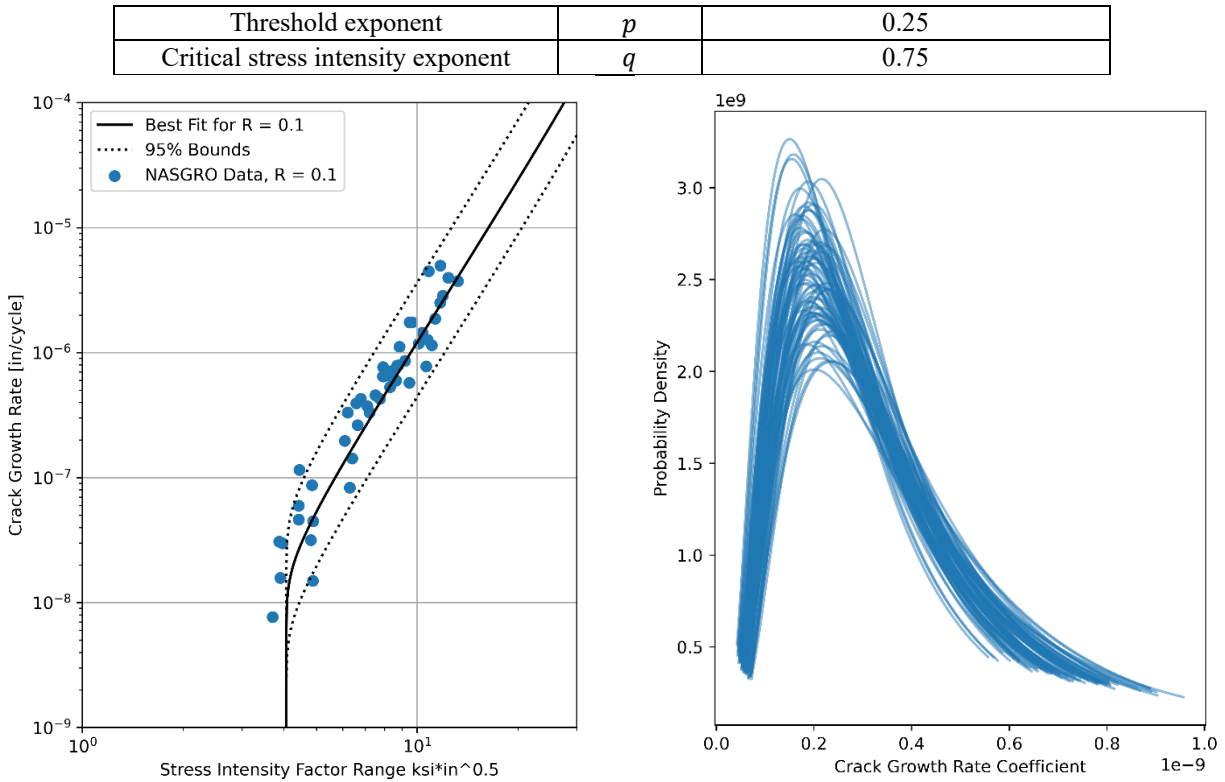
The crack growth rate was modeled as uncertain by fitting to crack growth rate data from the NASGRO material database for wrought Ti 3Al-2.5V. The crack growth model used in this assessment was the NASGRO equation with the form

$$\frac{da}{dN} = C\left(\frac{1-f}{1-R}\Delta K\right)^m \frac{\left[1 - \frac{\Delta K_{th}}{\Delta K}\right]^p}{\left[1 - \frac{K_{max}}{K_c}\right]^q}$$

where $\frac{da}{dN}$ is the crack extension per cycle, ΔK is the stress intensity factor range over one cycle, C is the crack growth rate coefficient, and m is the crack growth rate exponent. The crack growth rate coefficient C was modeled as uncertain using a lognormal distribution with a median of 3.0×10^{-10} and a shape parameter of 0.65. To account for epistemic uncertainty, the median and shape parameters were modeled using normal distributions with standard deviations of 0.3 and 0.05 respectively. Material properties such as strength, fracture toughness, and the other constants in the NASGRO equation were taken from the NASGRO materials database and are presented in Table 1.

Table 1. Material and crack growth rate properties used in example reliability assessment.

Property	Symbol	Value
Ultimate tensile strength	σ_{us}	125 ksi
Tensile yield strength	σ_{ys}	105 ksi
Effective fracture toughness	K_{1e}	70 ksi$\sqrt{in}$
Crack growth rate coefficient	C	3.0E-10 (in/cycles)$\left(ksi\sqrt{in}\right)^{-m}$
Crack growth rate exponent	m	4.0

| Threshold exponent	p	0.25
Critical stress intensity exponent	q	0.75

Figure 13. Left: Best fit with 95% bounds to NASGRO crack growth rate data. Right: Spread resulting from epistemic uncertainty in crack growth rate coefficient.

Fatigue loading was modeled using cyclic axial and bending stresses applied to the tube. A random vibration spectrum was produced for each flight event besides proof testing. The median fatigue spectrum is shown in Table 2 and Figure 14. Uncertainty in loads was modeled using a scale factor on the cyclic load amplitude. The scale factor was modeled assuming the flight-to-flight uncertainty in vibration environment amplitude was normally distributed with a standard deviation of 2 decibels. This corresponds to a scale factor applied to the fatigue environment being lognormally distributed with a shape parameter equal to the natural log of 2. To prevent completely unrealistic results, bounds were also placed on this distribution to prevent the scale factor from exceeding ±8 dB.

Table 2. Median load spectrum 3σ peak loads per flight event used in example assessment.

| Flight Event	Static Tensile Stress [psi]	Static Bending Stress [psi]	Dynamic Tensile Stress [psi]	Dynamic Bending Stress [psi]	Apparent Frequency [Hz]	Duration [s]
Pressure Proof	6000	4000	N/A	N/A	N/A	N/A
Engine Hot Fire	500	300	300	3900	150	3
Static Fire Abort	500	400	200	3600	155	3
Static Fire	600	400	300	4700	155	3
Liftoff Abort	600	400	300	3200	175	3
Early Flight	700	400	400	4000	178	10
Mid Flight	700	400	400	3700	141	100
Engine Cutoff	600	400	300	3400	187	10
Early Reentry	100	100	400	12100	165	30
Late Reentry	500	100	300	12100	161	100
Recovery	400	100	200	9700	148	10
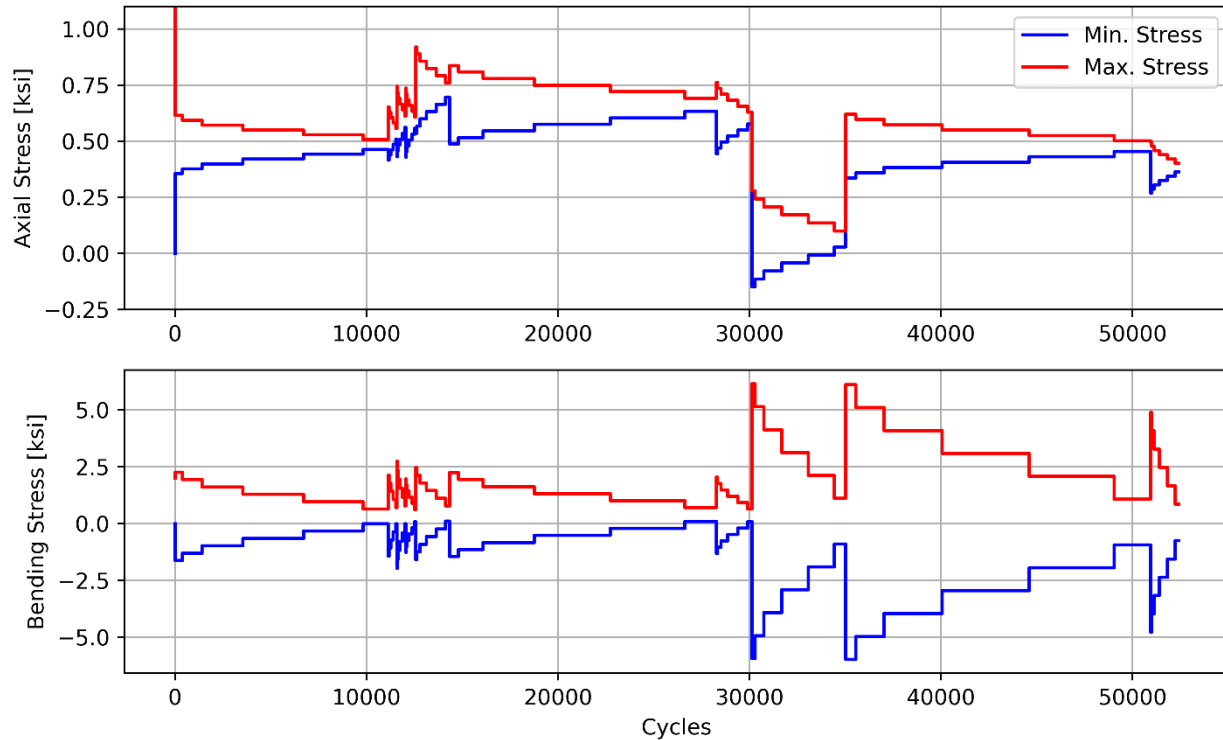
Figure 14. Median fatigue spectrum showing minimum (blue) and maximum (red) stress for each cycle. The cyclic stress amplitude is the difference between the maximum and minimum stress.

Initial flaws were assumed to be semi-elliptical circumferential surface cracks on the exterior of the tube with aspect ratio $a/c = 0.2$. The flaw orientation and aspect ratio are considered bounding assumptions because external circumferential cracks are the most sensitive to bending stresses. The initial flaw size was modeled as uncertain using a modified version of the exceedance curve from [7]. This flaw size distribution corresponds to the occurrence of hard alpha inclusions in titanium forgings and is used as example data only. The modified exceedance curve used in this assessment is shown in Figure 15 which encodes both the information that each tube had about a 10% chance of containing a flaw and the size distribution of those flaws. The flaw size distribution is non-parametric, so Monte Carlo sampling was performed using inverse transform sampling. This flaw size distribution was assumed to be bounding, so the epistemic uncertainty associated with the distribution was not directly modeled.

17
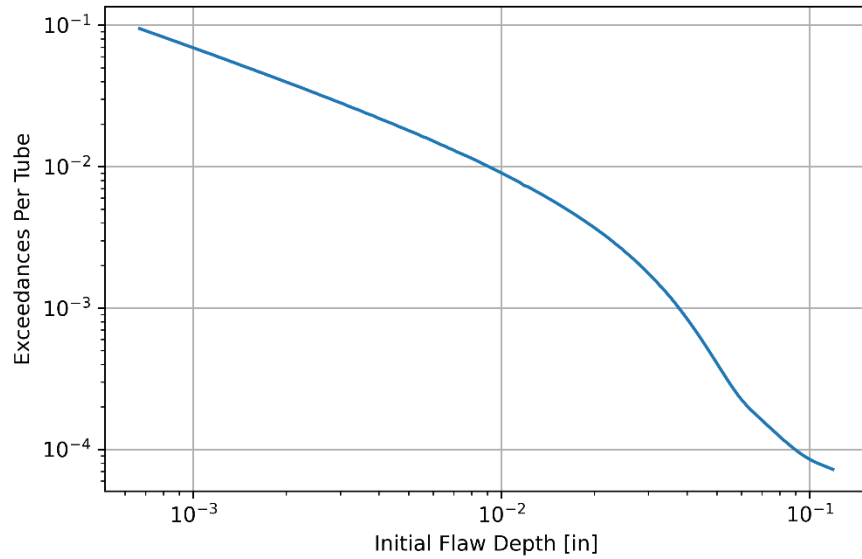
Figure 15. Modified exceedance curve used in example reliability assessment. The probability of any flaw occurring was 10% and the size distribution is encoded by the shape of the exceedance curve.

Finally, inspection simulation was performed to model the removal of tubes with detectable indications from the production flow. The POD curve in this assessment is shown in Figure 16. Inspection was simulated for each tube. If that tube contained a flaw, then the depth of that flaw determined the probability of detection from the POD curve. From there, a random number generator was used to determine if the flaw was detected or not. If a flaw was detected in a tube, then the tube was eliminated and replaced with a new sample. The POD curve in this example was assumed to be a bounding curve, such as the 95% confidence curve, so the epistemic uncertainty associated with it was not directly modeled.
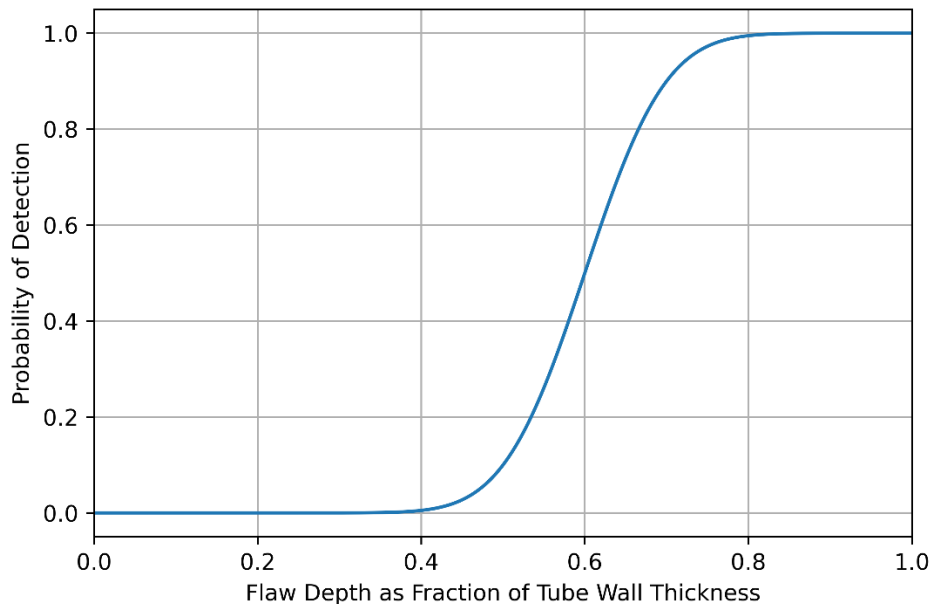

Figure 16. Probability of detection curve used in example assessment.

Using these distributions and the POD curve, the two-loop Monte Carlo assessment was performed. 100,000 aleatory realizations were simulated for each of 100 epistemic realizations. Each epistemic realization varied the distribution parameters for the tube wall thickness and the crack growth rate and produced one estimate of the probability of failure.

Figure 17 plots the cumulative probability of failure vs number of flights. Results at the 50% and 90% confidence level, tabulated in Table 3, were computed by taking the 50% and 90% quantiles of the probability of failure estimates for each flight. The epistemic uncertainty is represented by the spread between the blue curves. In this example, this spread could be reduced taking additional measurements of the tube wall thickness or testing additional crack growth rate samples to decrease the uncertainty in their distribution parameters.

Table 3. Cumulative probabilities of failure at 50% and 90% confidence.

Number of Flights	Cumulative Probability of Failure	
	50% Confidence	90% Confidence
10	8.78E-5	1.21E-4
20	2.29E-4	3.00E-4
30	3.96E-4	5.11E-4
40	6.02E-4	7.41E-4
50	8.11E-4	9.67E-4
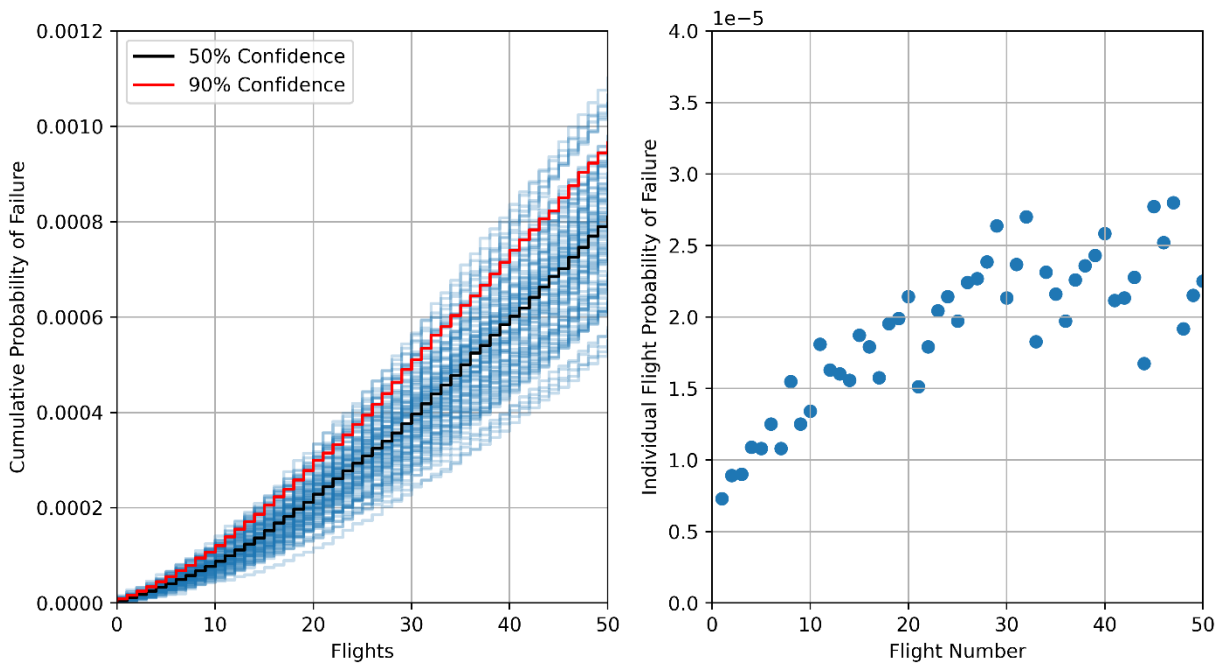
Figure 17. Tube cumulative probability of failure (left) and per-flight probability of failure (right) up to 50 flights.

The flight-by-flight probability of failure was computed by taking the numerical derivative of the 90% confidence cumulative data. These results represent the probability of failure for the next flight given that the part has survived all previous flights. In this example, the up until about flight 25, the next flight had a higher probability of failure previous flight. However, past that point, the probability of failure of each subsequent flight was approximately the same. The probability of failure should eventually begin to increase again as high-cycle fatigue becomes the dominant mode of failure. However, high-cycle fatigue was not modeled in this example.

As a point of comparison, the analysis was repeated using a DFM assessment. Mean wall thickness and median crack growth rate were used. The load amplitude of the median fatigue spectrum in Table 2 was increased to the P99 level

by applying a scale factor of 4.652 dB, based on the assumed standard deviation of 2 dB and the 99th percentile z-score of 2.326 for a normal distribution. Finally, the initial crack depth was based on the standard initial flaw size for radiographic inspection from [2], equal to 0.7 times the tube wall thickness. With these parameters and a life factor of 4, the DFM assessment predicted a damage tolerance life of only 1 flight. This life prediction could be extended by performing special NDE qualification to demonstrate reliable detection of smaller flaws.

B. Reliability Analysis of Additively Manufactured Stage Tank Cylinder

In the previous example, the flaw was assumed to be in the worst-case location. This example demonstrates the application of the reliability-based damage tolerance analysis with variable flaw location within a non-uniform stress field. An additive manufactured tank is considered because defects are more likely to be introduced throughout the tank, while in traditional manufacturing flaws are more likely to be concentrated in welded areas.

The reliability-based damage tolerance method was used to predict the probability of failure versus number of flights for an additively manufactured stage tank cylinder wall. The tank is made of an aluminum alloy and has a diameter of 72 in, a length of 350 in, and a nominal wall thickness of 0.125 in. The simulated tank is assumed to be manufactured using a wire-fed directed energy deposition (DED) process.

Tank wall thickness, crack growth rate, initial flaw size, flaw location, and number of flaws within the tank were treated as random variables. Distribution information for each of these input variables is shown in Table 4. For distributions with uncertain parameters, the parameters were modeled as Normal random variables with a standard deviation equal to the uncertainty value listed in the table. The parameters were sampled in the outer loop of the analysis.

Table 4. Parametric distributions used in example assessment.

Input Variable	Distribution Type	Distribution Parameters
Wall Thickness	Truncated Normal	$\mu = 0.125 \pm 0.004$ in $\sigma = 0.005 \pm 0.001$ in $a = 0.115$ in, $b = 0.135$ in
Crack Growth Rate Coefficient	Lognormal	$\mu^* = (5.0 \pm 1.0) \times 10^{-9}$ $s = 0.42 \pm 0.05$
Initial Flaw Depth	Pareto	$x_m = (1.728 \pm 1.047) \times 10^{-4}$ in $\alpha = 1.322 \pm 0.146$
Circumferential Flaw Location	Uniform	$a = 0$ deg, $b = 360$ deg
Number of Flaws Per Layer	Poisson	$\lambda = 10$

where μ is the Normal distribution mean, σ is the Normal distribution standard deviation, μ^* is the distribution median, s is the Lognormal distribution shape parameter, x_m is the Pareto distribution minimum value, α is the Pareto shape parameter, λ is the expected value of the Poisson distribution, and a and b are the lower and upper bounds respectively for bounded distributions.

The total number of flaws within the tank and their locations were determined through a simple simulation of the DED manufacturing process. The build of the tank was simulated layer-by-layer, with a layer height of 0.5 in for a total of 700 layers. Each layer produced a random number of flaws, governed by a Poisson distribution with an expected value of 10 flaws per layer. The Poisson distribution arises from the assumption that every incremental length of material deposited by the print head has a constant chance to produce a flaw. The circumferential position of the flaws throughout the layer was sampled from a Uniform distribution, and the axial position depends on the station height of the layer which the flaw occurred on.

Flaws were modeled as semi-circular external circumferential surface flaws. The flaw depth was sampled from a Pareto distribution with uncertain distribution parameters. This flaw size distribution combined with the number of flaws per layer produces the uncertain exceedance curve shown in Figure 18.
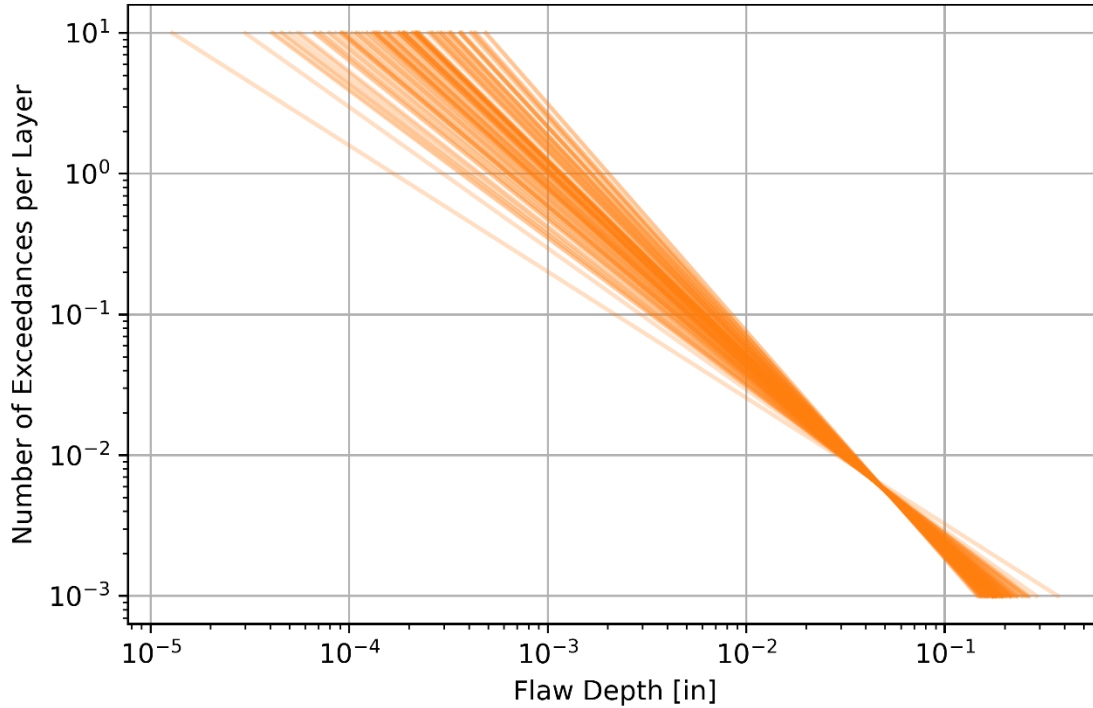
Figure 18. Uncertain flaw depth exceedance curve used in example assessment.

The tank is subjected to aero-loads during ascent and descent; and these loads contribute to the total fatigue load spectra. In addition to pressure loads from leak checks, proof test, and flight pressures, there are axial and bending stresses arising from flight. The load spectrum is shown in Table 5. During flight the bending stress and axial stress varies as a function of axial station. Figure 19 shows the spatial variation of bending stress. Axial stress throughout the tank was assumed to be uniform and bounding of the actual expected stress spatial variation. To determine the fatigue spectrum experienced by each flaw in the tank, the dynamic bending stress in Table 5 is multiplied by the normalized bending stress at the flaw location in Figure 19.

Table 5. Fatigue spectrum used in example assessment.

Flight Event	Static Tensile Stress [psi]	Static Bending Stress [psi]	Alternating Tensile Stress [psi]	Alternating Bending Stress [psi]	Number of Cycles
Pressure Proof	11,880	0	N/A	N/A	6
Pressure Cycling	10,800	0	N/A	N/A	24
Flight Cycles	10,800	0	400	12,600	1000
Leak Checks	10,800	0	N/A	N/A	8
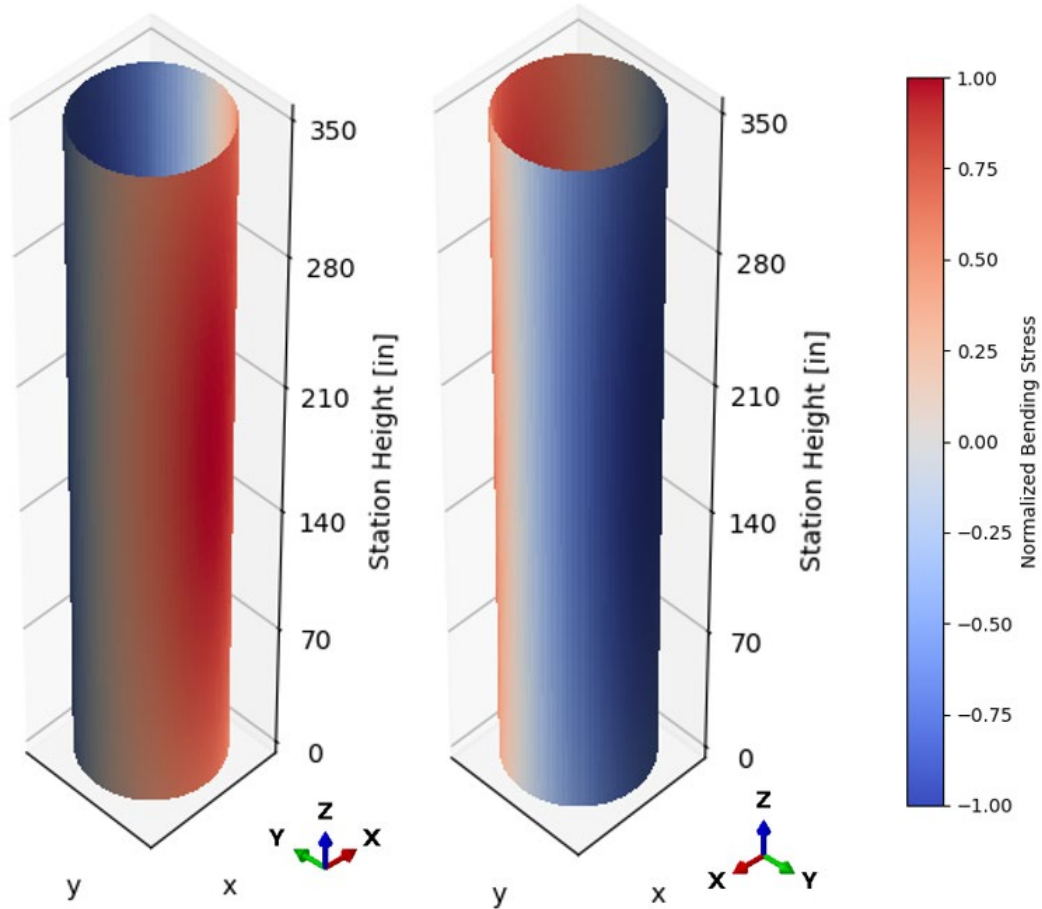
Figure 19. Spatial variation of bending stress across stage tank.

Inspection simulation was performed using the same POD curve as the previous example, Figure 16. When a flaw in the tank was detected, the flaw was removed from the tank to simulate a repair process. Results from the reliability-based damage tolerance assessment are shown in Figure 20.
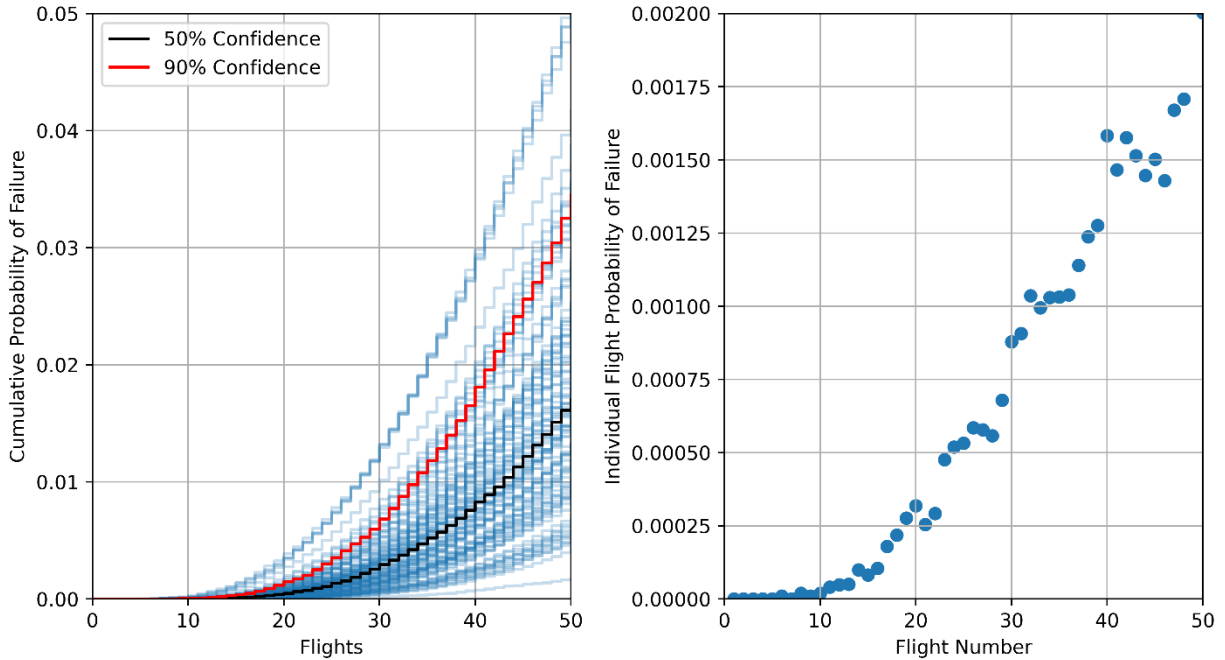
Figure 20. Stage tank cumulative probability of failure results (left) and per-flight probability of failure (right). The probability of failure of each successive flight is higher than the last.

The reliability results show that the predicted probability of failure of the tank barrel is 4×10^{-5} after 10 flights and 1.5×10^{-3} after 20 flights. As a comparison, a deterministic analysis was performed using the same fatigue spectrum along with the mean wall thickness, median crack growth rate, and a life factor of 4. The initial flaw size was based on the P90/C90 flaw size for radiographic inspection from [2], equal to 70% of the wall thickness. With these parameters, the deterministic assessment predicts a damage tolerance life of 8 flights. To extend service life with DFM, an approach is to develop a special NDE that can improve upon the minimum detectable flaw size or implement an in-situ monitoring technique that allows for real-time detection of voids and flaws.

C. Prediction of Additively Manufactured Coupon Fatigue Life

In [17], the application of reliability-based damage tolerance using probabilistic fracture mechanics and deterministic fracture mechanics was examined with an example problem of AM AlSi10Mg round bar coupons under cyclic axial loading conditions, Figure 21. In that study, the statistical distributions for flaw population, size, location, and variation of fracture properties were informed from three previously published studies. The probabilistic damage tolerance approach underpredicted mean cycles to failure and the variability in cycles to failure compared to test. However, the number of cycles to failure at four 9's of reliability and from deterministic analysis with a factor of four bounded all test measurements, see Figure 23. A parametric study showed that reducing AM porosity can increase service life but may have only a small impact if high reliability is required.
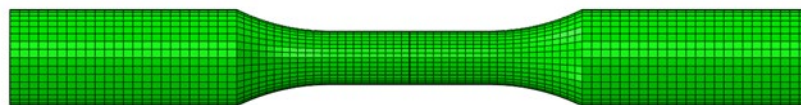
Figure 21. Geometry of round bar fatigue specimen.
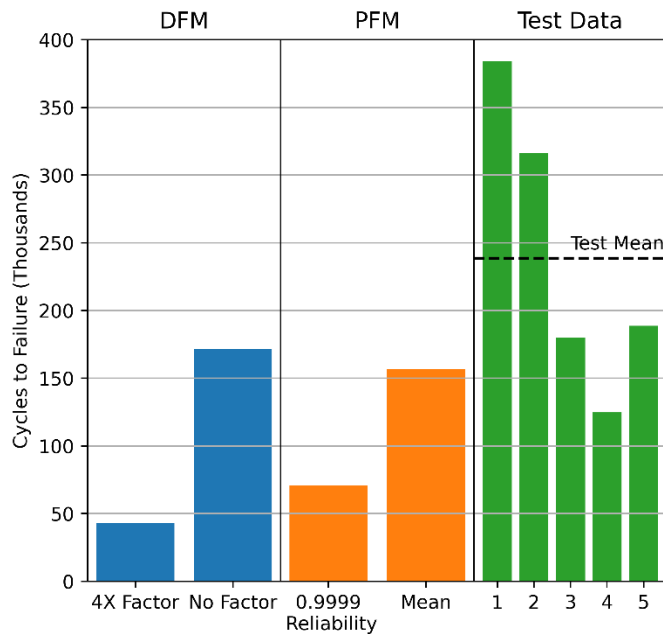
Figure 22. Comparison of PFM and DFM fatigue life predictions against fatigue test data.

VII. Summary

A framework for applying reliability-based damage tolerance to space structures was presented as a method to meet the service life demands of highly reusable launch and space vehicle systems. The framework consists of three components: the characterization of uncertainty in the input variables, the propagation of uncertainty through a fracture analysis, and the analysis of the output uncertainty.

The key input variables include material properties, geometry, loads, inspection probability, and defect characteristics among others. Recommendations were provided to collect the required data to characterize the uncertainty in each variable. Propagation of the input uncertainty through a fracture analysis was performed using a two-loop Monte Carlo sampling approach which maintains separation between the aleatory and epistemic uncertainty to compute the probability of failure and confidence level.

This approach was applied to two example assessments: a plumbing tube section subjected to a random vibration environment and a launch vehicle stage tank subjected to internal pressure and flight loads. These examples demonstrated the probability of failure calculation over several flights.

References

[1] NASA-STD-5019A w/change 3, "Fracture Control Requirements for Spaceflight Hardware", NASA Technical Standards, standards.nasa.gov, 2020. https://standards.nasa.gov/standard/NASA/NASA-STD-5019

[2] NASA-STD-5009B, "Nondestructive Evaluation Requirements for Fracture Critical Metallic Components," NASA Technical Standards, standards.nasa.gov, 2019. https://standards.nasa.gov/standard/NASA/NASA-STD-5009

[3] Parker, P. A., Koshti, A. Forsyth, D. S., Suits, M. W., Walker, J. L., Prosser, W. H., "A Survey of NASA Standard Nondestructive Evaluation (NDE)," NASA Langley Research Center, NASA/TM-20220013820, Sept. 2022. https://ntrs.nasa.gov/citations/20220013820

[4] S. Rahman, "Probabilistic fracture mechanics: J-estimation and finite element methods," Engineering Fracture Mechanics, vol. 68, no. 1, pp. 107–125, Jan. 2001, doi: https://doi.org/10.1016/s0013-7944(00)00092-8.

[5] Y.-T. . Wu, M. Enright, H. Millwater, G. Chell, C. Kuhlman, and G. Leverant, "Probabilistic methods for Design Assessment of Reliability with Inspection (DARWIN)," 41st Structures, Structural Dynamics, and Materials Conference and Exhibit, Apr. 2000, doi: https://doi.org/10.2514/6.2000-1510.

[6] R. McClung et al., "Integration of Manufacturing Process Simulation with Probabilistic Damage Tolerance Analysis of Aircraft Engine Components," 53rd AIAA/ASME/ASCE/AHS/ASC Structures, Structural Dynamics and Materials Conference
20th AIAA/ASME/AHS Adaptive Structures Conference
14th AIAA, Apr. 2012, doi: https://doi.org/10.2514/6.2012-1528.

[7] FAA Advisory Circular 33.14-1 Change 1, "Damage Tolerance for High Energy Turbine Engine Rotors," Federal Aviation Administration, Mar. 2017.

[8] FAA Advisory Circular 33.70-1 Change 1, "Guidance Material for Aircraft Engine Life-Limited Parts Requirements," Federal Aviation Administration, Feb. 2017

[9] NRC RG 1.245, Revision 0, "Preparing Probabilistic Fracture Mechanics Submittals," U.S. Nuclear Regulatory Commission, nrc.gov, Jan. 2022.

[10] NRC NUREG/CR-7278, "Technical Basis for the use of Probabilistic Fracture Mechanics in Regulatory Applications," U.S. Nuclear Regulatory Commission, nrc.gov, Jan. 2022. https://www.nrc.gov/reading-rm/doc-collections/nuregs/contract/cr7278/index.html

[11] Manning, S. D., "USAF Durability Design Handbook: Guidelines for the Analysis and Design of Durable Aircraft Structures," Air Force Systems Command, January 1984

[12] Johnson, W. S., "The history, logic, and uses of the Equivalent Initial Flaw Size approach to total fatigue life prediction.", Procedia Engineering, vol. 2 no. 1, p. 47-58, April 2010, doi: https://doi.org/10.1016/j.proeng.2010.03.005

[13] Lemons, R., A., Quate, C. F., "Acoustic microscope—scanning version," Applied Physics Letters, vol. 24 p. 163-165, 1974, doi: https://doi.org/10.1063/1.1655136

[14] Maire, E., Withers, P. J., "Quantitative X-ray tomography," International Materials Reviews, vol. 59, no. 1, p. 1-43, doi: https://doi.org/10.1179/1743280413Y.0000000023

[15] SMC Standard SMC-S-016, "Test Requirements for launch, Upper-Stage, and Space Vehicles," Air Force Space Command, September 2014.

[16] Hoffman, F. O., Hammonds, J. S., "Propagation of Uncertainty in Risk Assessments: The Need to Distinguish Between Uncertainty Due to Lack of Knowledge and Uncertainty Due to Variability," Risk Analysis, vol. 14 no. 5, p. 707-712, Oct. 1994, https://doi.org/10.1111/j.1539-6924.1994.tb00281.x.

[17] Qu X., Shimizu, L., Rome, J., Nordendale, N., Goyal, V., "Reliability-Based Damage Tolerance of Additive Manufacturing Parts," NAFEMS World Congress, May 2023.